JACS
JOURNAL OF THE AMERICAN CHEMICAL SOCIETY
Communication
pubs.acs.org/JACS

Distance Dependence of the Photocatalytic Efficiency of TiO_2 Revealed by in Situ Ellipsometry

Adrián Carretero-Genevrier, Cédric Boissiere, Lionel Nicole, and David Grosso*

Laboratoire Chimie de la Matière Condensée de Paris, UMR UPMC-Collège de France-CNRS 7574, Collège de France, 11 place Marcelin Berthelot, 75231 Paris, France

Supporting Information

ABSTRACT: Spectroscopic ellipsometry was utilized to follow in situ photodegradation of organic species in the vicinity of TiO_2 nanoparticles during UV irradiation. Stacked layers composed of TiO_2, mesoporous SiO_2, and mixed mesoporous SiO_2/TiO_2 nanocomposites with controlled thickness and porosity were used as model materials. Lauric acid molecules and poly(vinyl chloride) (PVC) layers were used as model mobile and immobile pollutants, respectively. The local photocatalytic activity was deduced by monitoring the variation of the thickness and refractive index of each independent layer. We show that the photocatalyzed degradation of an organic pollutant takes place only when the latter is located in close vicinity to the TiO_2 nanoparticle surface or can naturally diffuse toward it. As a result, the reaction efficiency is directly related to the organic pollutant diffusion. We also show that the distance of photocatalysis efficiency (d_s) at which radical intermediates are still present and active is <10 nm from the TiO_2 surface under the conditions of the experiments. This was confirmed by the fact that an immobile condensed organic phase such as PVC was protected from the photocatalytic degradation when separated from the TiO_2 by a 20 nm layer of mesoporous silica.

Because of its exceptional intrinsic physical chemical properties, TiO_2 has been extensively studied as potential material to be used in photocatalysis,[1−4] as self-cleaning optical coatings,[5,6] for solar energy conversion,[7,8] for energy storage,[9] or in sensing.[10] Among these, photocalytic degradation of organic species is a hot topic, and a number of investigations are still being conducted today to provide a better understanding of the multistep mechanism in order to improve self-cleaning and air purification efficiency.[11] This photoactivity is associated with the transformation of electromagnetic energy into electron−hole pairs in the conduction and valence bands of TiO_2, which can then be scavenged by surface oxygen-based trapping groups. The overall quantum efficiency for interfacial charge transfer is function of the delicate competition between charge-carrier recombination and trapping (from pico- to nanoseconds) followed by trapped-charge-carrier recombination and surface charge transfer (from micro- to milliseconds),[1,12,13] which are governed by the structure, the dimension, the morphology, and the arrangement of the primary TiO_2 nanoparticles. It is now common knowledge that systems composed of anatase nanoparticles in the range from 5 nm to several tens of nanometers in diameter are the most active.[14] Upon irradiation at energies higher than 3.5 eV, Ti−$OH^•$ radicals can be formed by electron transfer into the TiO_2 valence band, while $O_2^{•−}$ radical anions are created when adsorbed O_2 molecules gain electrons from the conduction band. These two types of radicals are primary electron acceptors and donors, respectively, initiating the secondary reactions with water that lead to activated oxygen species, such as $HOO^•$ or $OH^•$. These radicals, including Ti−$OH^•$ and adsorbed $O_2^{•−}$, are responsible for the degradation of nearby organic species. Recent reports have shown that when TiO_2 nanoparticles are combined with SiO_2 into nanocomposites, the photoactivity is still efficient[5,6] and can be even higher than that of pure Degussa P25 reference materials,[15] suggesting that radicals could be found and be active away from the TiO_2 surface. However, it is sensible to state that because of their short lifetimes, their concentrations decrease with increasing distance from the semiconductor surface. Consequently, one expects the decomposition rate of a given pollutant to decrease when its distance from the TiO_2 surface increases. As a result, how far from the TiO_2 surface one can still find active radicals for a given environment and specific conditions is a crucial question for the optimization of the next generation of photocatalysts.

In other words, the distance of catalytic efficiency (d_s), that is, the critical distance at which an immobilized organic moiety remains safe from those diffused radicals, is crucial. This consideration becomes of utmost importance in the design of multifunctional hybrid systems for which photocatalysis is to be combined with an organic function or a polymeric organic phase. In these cases, the organic phase can be protected from radical intermediates if localized and immobilized at a distance from the TiO_2 surface that is greater to d_s. To estimate d_s, one must be able to detect radicals at distances of <100 nm from the TiO_2 surface. Since it is very difficult to obtain this information directly, in this work we used an indirect method based on real-time spectroscopic ellipsometry investigations.[16] To do so, we designed a model multilayer optical platform typically composed of a porous anatase nanoparticulate TiO_2 layer and an intercalated mesoporous silica layer, which were prepared by the evaporation-induced self-assembly (EISA) method[17,18] (see Figure 1). The thicknesses and porosities of the two films can be independently and accurately adjusted

Received: April 2, 2012
Published: June 18, 2012

dx.doi.org/10.1021/ja303170h | J. Am. Chem. Soc. 2012, 134, 10761−10764

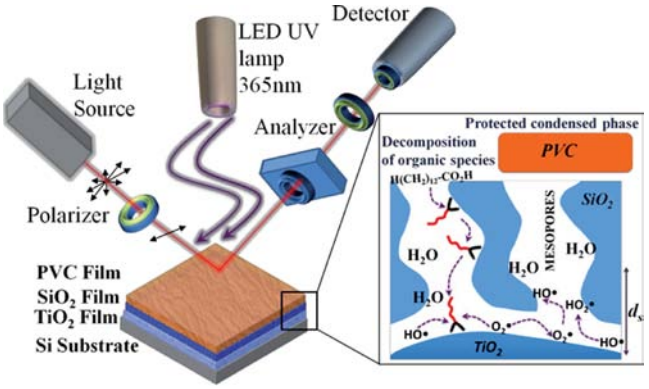

Figure 1. Experimental scheme of the ellipsometric setup designed to monitor in real-time n and h of each individual layer of a stacked TiO_2/mesoporous SiO_2/PVC system during irradiation with a UV LED source.

through chemical and processing conditions.[19] In this configuration, the silica layer is fully permeable, allowing radicals generated at the TiO_2 surface upon UV irradiation to diffuse within both films' pores. In addition, the pores of the silica layer can also be infiltrated with adsorbed mobile pollutant molecules that can freely diffuse toward the TiO_2 surface. In the latter case, the pollutant molecules are also found in the pores in the lower TiO_2 layer. Eventually, a third layer of polymer [e.g., poly(vinly chloride) (PVC)] can be deposited at the surface of the mesoporous silica or a mixed TiO_2/mesoporous SiO_2 layer. These stacked layer platforms are constructed in such a way that (i) each layer has a controlled thickness, (ii) each ceramic layer is porous and allows free accessibility and transport inside the pores, (iii) the organic species are spatially separated from the semiconductor surface by a distance that can be relatively accurately adjusted by the thickness of the silica layer or by the proportion of TiO_2 dispersed in the mixed layer, and (iv) one can simultaneously and independently follow the refractive index n and thickness h of each layer of the stack upon UV irradiation using the modified in situ ellipsometric system described in Figure 1. The photocatalytic activity is then deduced from the variation in n of the organically polluted ceramic layers or the variation in h of the PVC top layer. We show that d_s is <10 nm and that organic molecules must be able to diffuse within close vicinity of the TiO_2 surface, where radical species are highly concentrated, in order to be consumed. Second, a solid polymer can safely be combined with the TiO_2 photocatalyst as long as the two solid phases are separated by, under the present conditions, a barrier consisting of a 20 nm layer of mesoporous SiO_2.

The experiments were performed as follows. Absolute ethanol (EtOH) was purchased from Normapur. Tetraethylorthosilicate (TEOS) precursor, the nonionic surfactant Brij-56, and PVC were purchased from Sigma-Aldrich. A 13% (w/w) aqueous solution of 15 nm diameter anatase TiO_2 nanoparticles [Figures 1 and 2 in the Supporting Information (SI)] was purchased from Nanostructured & Amorphous Materials, Inc. TiO_2 films were prepared from this solution after dilution with 66% (v/v) EtOH. The films were deposited on silicon substrates by dip-coating at room temperature at a constant withdrawal rate of 4 mm·s^{-1} and then immediately thermally treated at 450 °C for 10 min in air. The thickness of the TiO_2 films was ~80 nm, while the refractive index at 700 nm (n_{700nm}) was measured to be 1.98. Mesoporous silica films were prepared from TEOS/Brij-56/H_2O/EtOH solutions with a molar ratio of 1:0.05:5:25. TEOS was first dissolved in a solution containing EtOH, 2 M HCl, and H_2O before addition of Brij-56. The resulting solution was stirred for at least 2 h before being deposited on silicon substrates by dip-coating at room temperature with a controlled relative humidity of 40%. The thickness of the silica layers was tuned by using different dipping rates (1, 2, and 4 mm·s^{-1}) while keeping the other dip-coating conditions constant. After coating, the films were immediately thermally treated at 450 °C for 10 min in air. The final mesoporous silica layers were transparent with n_{700nm} = 1.23. PVC films were prepared from solutions composed of PVC diluted in 50% (v/v) acetone. The films were deposited by dip-coating at room temperature and immediately cross-linked at 130 °C for 15 min. The film structure was investigated using field-emission gun scanning electron microscopy (FEG-SEM) on a Hitachi SU6600 instrument. Grazing-incidence small-angle X-ray scattering (GISAXS), performed on a Rigaku S-max 3000 instrument equipped with a microfocus source (λ = 0.154 nm) and a 2D Gabriel-type detector placed 1480 mm from the sample (incidence angle = 0.2°), was used to assess the mesostructure of the films. Diffraction patterns were analyzed using Igor software version 13. Ellipsometry measurements were performed on a UV−vis (240−1000 nm) variable-angle spectroscopic ellipsometer (VASE; Woollam 2000U), and the data analysis was performed with Wvase32 software using Cauchy models in the visible range. The photoactivity of the systems was investigated by following both the refractive index of the layer containing lauric acid and the thickness of the PVC layer upon UV irradiation. Lauric acid was infiltrated into the stacked layers by dip-coating them in a saturated ethanolic solution. The excess lauric acid deposited at the surface of the system was wiped away using a wet tissue. These polluted samples were placed in air at a distance of 5 cm under a UV lamp based on 250 mW Nichia NCSU033A 365 nm UV light-emitting diode (LED), and the optical density was recorded every minute using the previous ellipsometry conditions over a period of up to 2 days.

The first system studied was a bilayer composed of a 70 nm thick mesoporous silica layer deposited on the surface of a 90 nm thick layer of TiO_2 nanoparticles. SEM images of the bilayer are shown in Figure 2a,b. The top surface of the mesoporous silica layer shows a hexagonal organization of 3−4 nm diameter pores (Figure 2b). The inset shows the related GISAXS pattern, which confirms the typical contracted body-centered cubic *Im3m* organization of pores with domains having their [110] direction normal to the surface. Under those conditions, pores are expected to be 3D-interconnected and open to both TiO_2 and air interfaces, allowing adsorbed molecules to diffuse freely within the pores by natural adsorption and chemical exchanges.

The system was then infiltrated with lauric acid, resulting in increases in the refractive indices for both the top silica layer and the bottom titania layer, from 1.25 to 1.36 and from 1.97 to 2.07 respectively. These confirmed the presence of the organic pollutant within the pores. The variations in the refractive index were monitored using ellipsometry during UV exposure (Figure 2c). For comparison, the same protocol was applied to a single mesoporous SiO_2 layer. After 5 h of irradiation, the refractive index of the mesoporous SiO_2 (single layer) remained constant, confirming that lauric acid was not decomposed by photochemistry without the presence of nearby titania. In the bilayer system, the thickness of each layer did not change upon irradiation, but the refractive indices of both the top and

dx.doi.org/10.1021/ja303170h | J. Am. Chem. Soc. 2012, 134, 10761−10764

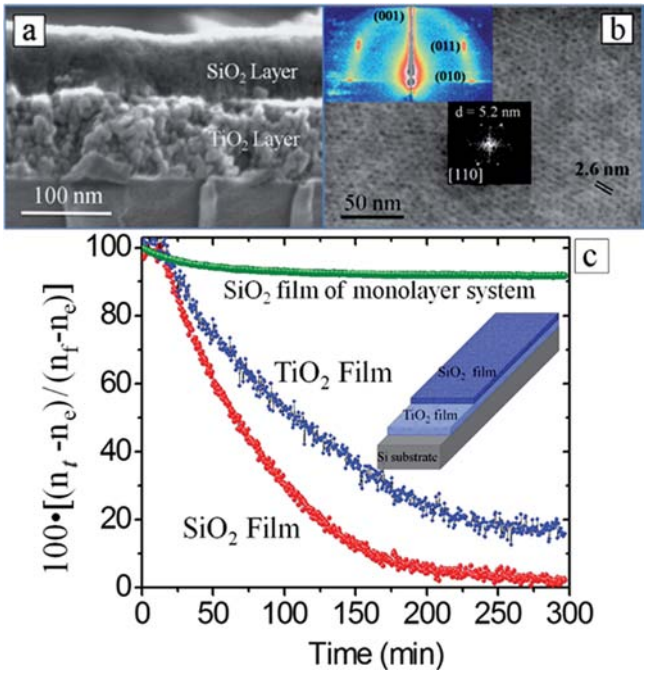

Figure 2. (a, b) FEG-SEM images of the TiO_2/SiO_2 bilayer: (a) cross section; (b) top surface. The insets in (b) display the corresponding fast Fourier transform (center) and 2D GISAXS pattern showing the typical diffraction peak of the *Im3m* mesostructure (upper left). (c) Variation of the quantity of lauric acid upon irradiation at 365 nm for both the TiO_2 (blue) and mesoporous SiO_2 (red) layers in the bilayer system and for the SiO_2 mesoporous layer of the monolayer system (green). The quantity of lauric acid is given by $100\cdot[(n_t - n_e)/(n_f - n_e)]$, where n_t, n_e, and n_f are the refractive indices of the layer at time t, the empty layer, and the layer fully infiltrated with lauric acid ($t = 0$), respectively.

bottom layers progressively decreased, reaching the refractive indices of the empty layers (n_e) after 5 h. This indicates efficient photocatalytic activity not only for pollutants that are located in the pores of the TiO_2 film but also for pollutants within the pores of the silica layer. Since the active species (e.g., $HOO^{\bullet}$, $OH^{\bullet}$, $O_2^{\bullet-}$) are created at the surface of the semiconductor, it is clear that the latter coexist with lauric acid in the pores. Contrary to what is usually reported for the standard decomposition of model molecules in solution, the rate of decomposition was not constant but instead decreased progressively with the consumption of the pollutants in the dry porous films. This reveals that the decomposition mechanism is limited by diffusion, since the quantum efficiency of the TiO_2 materials is expected to remain constant. The diffusion-limited nature of the reaction is evidenced by the linear decrease in the refractive index versus $t^{1/2}$ (SI Figure 4). The diffusion can be either that of the pollutants toward the semiconductor surface, that of the free activated species toward the pollutants, or both simultaneously. Interestingly, the rate of lauric acid decomposition was higher in the top silica layer than in the bottom titania layer. This can be explained if one assumes that the pollutants are degraded in the close vicinity of TiO_2 in the bottom layer and that a net flux of lauric acid is established from the top SiO_2 layer to the bottom TiO_2 layer, the latter being proportional to the difference in concentration and surface affinity. The net flux is thus expected to be progressively reduced with the diminution of the total amount of pollutant. In addition, one clearly remarks that while the top SiO_2 layer regains its empty state, the bottom TiO_2 layer has a final refractive index 20% higher than n_e. This higher density can be attributed to the trapping of carbonated residues of the photoinduced decomposition of lauric acid, which are known to form stable coordination bonds with the TiO_2 surface. It is clear that under these conditions the photocatalytic efficiency depends on the diffusion of the pollutants toward the radicals at the surface of TiO_2. However, to provide a better assessment of d_s, which is associated with the lifetime of the radicals, we performed the same investigation on a system where only the radicals are mobile, while the organic species cannot diffuse toward the TiO_2 surface. In this new $PVC/SiO_2/TiO_2/Si$ platform, a PVC layer was deposited onto the silica coating (Figure 3a). The PVC macromolecules could not penetrate

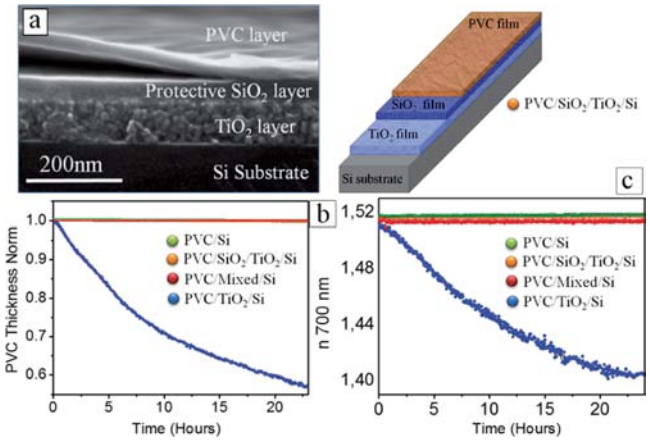

Figure 3. (a) SEM image of a cross section of a trilayer system composed of a PVC layer deposited on the mesoporous silica layer of a typical silica/titania bilayer. (b, c) Evolution of the refractive index and thickness of the 30 nm PVC layer in each of the four systems during UV irradiation. The thickness of the mesoporous silica layer was 20 nm.

inside the pores of the silica layer, as confirmed by the fact that the refractive index of the silica layer remained equal to n_e (1.25). In the following experiment, the thicknesses of the PVC, mesoporous SiO_2, and TiO_2 layers were adjusted to 30, 20, and 80 nm respectively, forcing radicals created at the TiO_2 surface to cross 20 nm of connected mesopores through silica before reaching the PVC surface. For comparison, two other systems were prepared and submitted to the same experiment: a single PVC layer deposited on a silicon wafer (PVC/Si) and a PVC layer deposited onto the TiO_2 single layer ($PVC/TiO_2/Si$). The evolution of the refractive index and thickness of the PVC layer upon UV irradiation for the three systems is shown in Figure 3b,c. One observes first that the refractive index and the thickness of the PVC layer in the PVC/Si system did not change significantly, suggesting that the PVC is relatively stable under the applied UV conditions. On the other hand, when directly in contact with the TiO_2 layer, the refractive index and the thickness of the PVC layer decreased considerably (from 1.52 to 1.40 and to 50% of the initial thickness, respectively) after 24 h of UV exposure. The decrease in refractive index indicates the creation of porosity within the PVC layer, suggesting that the photocatalytic decomposition not only takes place at the PVC−TiO_2 interface but also within the PVC layer through the diffusion of the radicals within the layer. This diffusion is made possible by the presence of natural defects (cracks, pores) in the film. Interestingly, when a 20 nm layer of

dx.doi.org/10.1021/ja303170h | J. Am. Chem. Soc. 2012, 134, 10761−10764

mesoporous silica was intercalated between the PVC and the titania layer, no noticeable decomposition of the polymer layer was observed, confirming that d_s through a mesoporous SiO_2 layer is less than its physical thickness (20 nm).

Here, despite the fully interconnected pores, radical intermediates never reached the PVC interface as a result of the shortness of their lifetime and possible deactivation taking place in contact with the silica suface. For further investigation of the protecting role of the mesoporous silica, the PVC layer was deposited on top of a 70 nm thick nanocomposite layer composed of 44% (v/v) TiO_2 nanoparticles randomly dispersed into the mesoporous silica matrix (SI Figure 3a,b).[6] When such a "mixed" film was artificially polluted with lauric acid, the latter was easily decomposed after 5 h of irradiation (SI Figure 3c), suggesting that the pores are fully open and that efficient radical species are created at the surface of the particles. In the same PVC/mixed/Si stack, the PVC layer interface was estimated to be <10 nm from the first TiO_2 nanoparticle (SI Figure 3b). The PVC refractive index and thickness evolutions are reported in Figure 3b,c, and here again, no significant variation was observed upon UV irradiation. The latter result confirms that diffusing organic species are decomposed by photocatalysis, while an immobile organic phase can be protected from radicals by a porous silica layer even when located very close to the semiconductor surface.

In summary, ellipsometry was found to be a very useful tool in assessing the local photocatalysis activity at the surface of TiO_2 films, and we used it to study different stacked layer systems of sintered TiO_2 nanoparticles, mesoporous silica, mixed mesoporous silica/TiO_2, and PVC films prepared by dip-coating. Many more complicated systems could also be envisioned and prepared by this approach for further investigations. We have shown that one can easily assess the distance of photocatalysis efficiency, d_s, which is the critical distance from the semiconductor surface at which radical intermediates are still present and active. Under the present conditions, where the medium was a mesoporous silica material, d_s was found to be <10 nm. The immediate consequence of this is that any condensed organic phase can be protected from photocatalytic degradation when located at a distance d_s > 10 nm from the semiconductor surface.

■ ASSOCIATED CONTENT

Supporting Information

Structural and physical characterization and photocatalytic activity of mixed layers. This material is available free of charge via the Internet at http://pubs.acs.org.

■ AUTHOR INFORMATION

Corresponding Author

david.grosso@upmc.fr

Notes

The authors declare no competing financial interest.

■ ACKNOWLEDGMENTS

We acknowledge COMPHOSOL2 (Fond Unique Interministériel dans le cadre du 9eme AAP) for financial support and IMPC for use of FEG-SEM facilities.

■ REFERENCES

(1) Hoffmann, M. R.; Martin, S. T.; Choi, W.; Bahnemann, D. W. *Chem. Rev.* **1995**, *95*, 69.
(2) Bouras, P.; Stathatos, E.; Lianos, P. *Appl. Catal., B* **2007**, *73*, 51.
(3) Sakatani, Y.; Grosso, D.; Nicole, L.; Boissière, C.; Soler-Illia, G. J. d. A. A.; Sanchez, C. *J. Mater. Chem.* **2006**, *16*, 77.
(4) Serpone, N. Photocatalysis. In *Kirk-Othmer Encyclopedia of Chemical Technology*; Wiley: New York, 2000.
(5) Faustini, M.; Nicole, L.; Boissiere, C.; Innocenzi, P.; Sanchez, C.; Grosso, D. *Chem. Mater.* **2010**, *22*, 4406.
(6) Gohin, M.; Allain, E.; Chemin, N.; Maurin, I.; Gacoin, T.; Boilot, J. *J. Photochem. Photobiol., A.* **2010**, *216*, 142.
(7) Erickson, D.; Sinton, D.; Psaltis, D. *Nat. Photonics* **2011**, *5*, 583.
(8) Grätzel, M. *Acc. Chem. Res.* **2009**, *42*, 1788.
(9) Leroux, F.; Dewar, P. J.; Intissar, M.; Ouvrard, G.; Nazar, L. F. *J. Mater. Chem.* **2002**, *12*, 3245.
(10) Palomares, E.; Vilar, R.; Green, A.; Durrant, J. *Adv. Funct. Mater.* **2004**, *14*, 111.
(11) Michael, A. H. *Surf. Sci. Rep.* **2011**, *66*, 185.
(12) Schindler, K. M.; Kunst, M. *J. Phys. Chem.* **1990**, *94*, 8222.
(13) Kamat, P. V. *Chem. Rev.* **1993**, *93*, 267.
(14) Chen, X.; Mao, S. S. *Chem. Rev.* **2007**, *107*, 2891.
(15) Dong, W.; Lee, C. W.; Lu, X.; Sun, Y.; Hua, W.; Zhuang, G.; Zhang, S.; Chen, J.; Hou, H.; Zhao, D. *Appl. Catal., B* **2010**, *95*, 197.
(16) Remillard, J. T.; McBride, J. R.; Nietering, K. E.; Drews, A. R.; Zhang, X. *J. Phys. Chem. B* **2000**, *104*, 4440.
(17) Grosso, D.; Cagnol, F.; Soler-Illia, G. J. d. A. A.; Crepaldi, E. L.; Amenitsch, H.; Brunet-Bruneau, A.; Bourgeois, A.; Sanchez, C. *Adv. Funct. Mater.* **2004**, *14*, 309.
(18) Brinker, C. J.; Lu, Y.; Sellinger, A.; Fan, H. *Adv. Mater.* **1999**, *11*, 579.
(19) Faustini, M.; Louis, B.; Albouy, P. A.; Kuemmel, M.; Grosso, D. *J. Phys. Chem. C* **2010**, *114*, 7637.

■ NOTE ADDED AFTER ASAP PUBLICATION

The version published ASAP on June 20, 2012 contained an error in the final paragraph. The corrected version reposted on June 21, 2012.